P2R-Net: Physics-to-Reality SM Calibration Network with Sparse Measurement Guidance for High-Precision MPI Reconstruction

Lizhi Zhang[1,†], Jintao Li[1,†], Hongbo Guo[1], Zijian Tang[1], Yinong Cui[1], Haoyu Pan[2], and Xiaowei He[1,*]

[1] School of Electronic Information (School of Artificial Intelligence), Northwest University, Xi'an, 710127, China
[2] Institute of Artificial Intelligence, Shenzhen University of Advanced Technology, Shenzhen 518107, China.
[†] Co-first Author; * Corresponding Author: hexw@nwu.edu.cn.

Abstract. Magnetic Particle Imaging (MPI) enables highly sensitive and rapid mapping of magnetic nanoparticle distributions, yet its image quality critically depends on accurate system matrix (SM) calibration. Conventional SM acquisition requires exhaustive full-volume measurements and is time-consuming, while purely physics-based SM simulators often deviate from real measurements due to simplifying assumptions and imperfect system characterization. To overcome these limitations, we propose P2R-Net, a Physics-to-Reality SM Calibration Network for High-Precision MPI Reconstruction. It is realized as a dual-branch encoder–decoder architecture, which integrates sparse measurement guidance with dense, idealized SMs generated from anisotropic magnetization model. The Multi-scale cross-attention aligns physics-domain representations with measurement-domain characteristics, preserving physical plausibility while adapting to real acquisition conditions. In addition, It incorporates Spatial shift convolution Block (SC-Block) to model SM spatial coupling and an Attention-Enhanced Feature Distillation (AFD) module to stabilize physics-derived features. Extensive experiments show that P2R-Net yields higher-fidelity SMs and improves downstream MPI reconstruction quality over state-of-the-art baselines, providing an efficient and practical alternative to time-consuming full-volume calibration. Code is available at https://github.com/lzclz/P2Rnet.git.

Keywords: Magnetic Particle Imaging · Deep Learning · System Matrix · Spatial Resolution · Physics-to-Reality Mapping

1 Introduction

Magnetic Particle Imaging (MPI) is a non-invasive modality that images the spatiotemporal distribution of superparamagnetic iron oxide nanoparticles with high sensitivity and rapid acquisition, enabling a broad range of preclinical applications such as angiography, cell tracking, cancer imaging, neuroimaging, and magnetic hyperthermia [21, 17, 23, 19]. As human-scale MPI scanners continue to mature, practical deployment increasingly depends on robust and efficient calibration and reconstruction pipelines.

Among existing reconstruction approaches, system-matrix (SM) based reconstruction remains the standard for achieving high image quality [13, 15]. However, obtaining a high-fidelity SM requires exhaustive calibration by measuring nanoparticle responses voxel-by-voxel across the field of view, which is prohibitively time-consuming (e.g., a $37 \times 37 \times 37$ calibration can take over 33.5 hours [3]) and must be repeated when acquisition settings, tracer properties, or magnetic conditions change [5, 20]. These constraints motivate research on accelerating SM acquisition while preserving quantitative accuracy for downstream MPI reconstruction.

Two main directions of Model-based SM generation and Measurement-based SM recovery have been explored. Model-based SM generation replaces measurements with physics-driven simulations using magnetization dynamics models, ranging from equilibrium and anisotropy-extended equilibrium formulations to more expressive but computationally demanding Fokker-Planck (FP) models [8, 1, 14]. Although physically grounded, purely simulated SMs often exhibit a domain gap to real measurements due to unmodeled system imperfections and complex field interactions. Measurement-based SM recovery instead reconstructs a dense SM from sparse measurements using interpolation, compressed sensing, or low-rank/tensor priors [11, 18, 4, 2, 6, 7]. More recently, deep learning has reframed SM recovery as a super-resolution problem by learning data-adaptive mappings from undersampled measurements to high-resolution SMs [3, 5, 22, 16]. While these learning-based methods improve sharpness and efficiency, they can still struggle with (i) the physics-measurement misalignment, (ii) insufficient modeling of MPI-specific spatial coupling and anisotropic response patterns, and (iii) distortion of response amplitudes and scaling that undermines quantitative reconstruction.

To address these limitations, we propose P2R-Net, a Physics-to-Reality mapping network for MPI system-matrix calibration. The core idea is to align a model-derived SM to the measurement domain using sparse measurements while preserving physical plausibility. P2R-Net takes a fully sampled model SM (magnetic dynamics prior) and an undersampled measured SM (system specific statistics) as inputs, and employs a dual-branch encoder–decoder with multi-scale cross-attention to inject measurement cues into the physics representation. In addition, we introduce structure-aware feature learning to explicitly model voxel-wise magnetic interaction coupling and support anisotropy-aware refinement, and further employ stabilized fusion to suppress error propagation and preserve quantitative correctness.

In summary, we make three contributions. (i) We propose a Physics-to-Reality mapping network with sparse measurement guidance for MPI system-matrix calibration, bridging physics-derived and undersampled measured SMs. (ii) We introduce structure-aware refinement via a shared SC-Block for voxel-wise coupling and an AFD module for bias correction and stable physics-consistent features. (iii) We realize the improvement of both SM resolution and downstream reconstruction quality, which enables denser and higher-fidelity MPI reconstructions than the original measurements in the unsupervised setting.

2 Method

2.1 Overview and Motivation

The motivation for our proposed scheme is rooted in the practical bottlenecks of SM based MPI reconstruction. The measurement model can be written in the linear from $\mathbf{u} = \mathbf{S}\mathbf{c}$. This inverse problem is ill-conditioned, and the reconstruction quality is highly sensitive to the fidelity of $\mathbf{S}$; However, fully sampling the field of view voxel-by-voxel is prohibitively time-consuming and must be repeated whenever acquisition settings, tracer properties, or magnetic conditions change. This tension between quantitative accuracy and calibration efficiency has become increasingly critical as human-scale MPI systems move toward routine deployment.

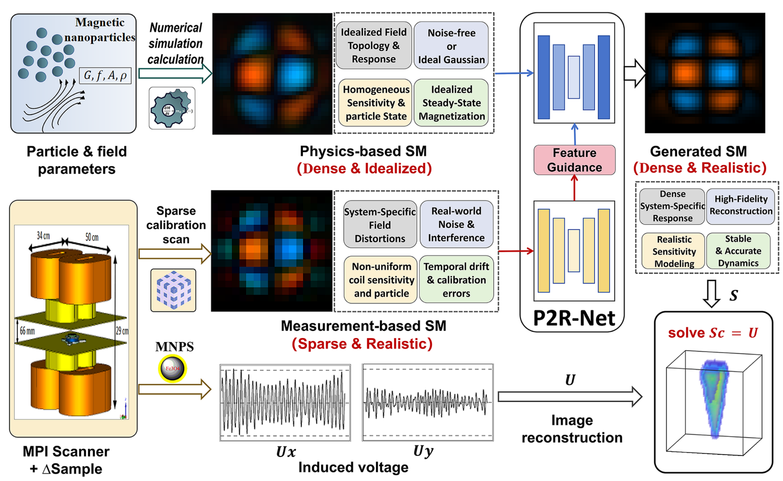

Fig. 1. The motivation and structure of the proposed method

As shown in Fig. 1, Physics-driven SM synthesis generates dense responses from magnetization models and yields globally coherent structure, yet it often leaves residual errors under hardware-dependent effects, field imperfections, and unmodeled interactions, leading to systematic mismatch in reconstruction [14]. Sparse-measurement SM recovery infers a full SM from limited real samples and reduces acquisition cost, but its accuracy depends strongly on the sampling strategy: MPI-specific spatial coupling and anisotropic response are difficult to extrapolate, and local amplitude/scale drifts can undermine quantitative consistency [3]. In short, physics-based synthesis is structurally strong but scanner-agnostic, whereas sparse recovery is scanner-specific but under-constrained.

To bridge this gap, we propose P2R-Net, a physics-to-reality mapping framework that uses a dense physics-based SM as the structural backbone and injects system-specific characteristics via sparse real measurements as guidance. Formally, the target high-fidelity SM is obtained by a conditional mapping:

$$\hat{\mathbf{S}}_{\mathrm{target}} = \Phi_{\mathrm{P2R}}(\mathbf{S}_{\mathrm{model}} \,|\, \mathcal{F}_{\mathrm{guide}}(\mathbf{S}^{\mathrm{sparse}}_{\mathrm{measure}}))\,, \tag{1}$$

where $\mathbf{S}_{\mathrm{model}}$ encodes global physical topology, and $\mathcal{F}_{\mathrm{guide}}(\cdot)$ extracts a compact reality-aware embedding from sparse measurements to steer the refinement toward the true system response.

2.2 Adaptive Truncation Anisotropic Equilibrium Model

To obtain a dense yet efficient physics prior for P2R-Net, we develop an Adaptive Truncation Anisotropic Equilibrium magnetization model. Standard Langevin-based equilibrium models typically neglect particle anisotropy and/or rely on fixed-order approximations, which either introduce modeling bias or incur prohibitive cost when constructing frequency-domain system matrices (SMs). Our model explicitly accounts for anisotropy while *adaptively* selecting the necessary high-order components to preserve nonlinear responses.

Specifically, we employ an anisotropic equilibrium formulation that incorporates the easy axis $\mathbf{n} \in \mathbb{S}^2$ and anisotropy strength $\alpha_{K_{\mathrm{anis}}}$. The system function $s_\ell(\mathbf{r}, t)$, defined as the temporal derivative of the mean magnetic moment $\overline{\mathbf{m}}$, is given by

$$s_\ell(\mathbf{r}, t) = \mu_0 m_0 p^R(\mathbf{r}) \frac{\partial}{\partial t} \left[\mathcal{E}\left(\beta \mathbf{H}(\mathbf{r}, t), \alpha_{K_{\mathrm{anis}}}(\mathbf{r}), \mathbf{n}(\mathbf{r})\right)\right], \tag{2}$$

where μ_0 is the vacuum permeability, m_0 denotes the magnetic moment magnitude, $p^R(\mathbf{r})$ is the receive coil sensitivity, $\mathbf{r}$ and t denote the spatial position and time, respectively, $\mathbf{H}(\mathbf{r}, t)$ is the applied magnetic field, β is the thermal scaling factor that normalizes the magnetic field strength, $\mathcal{E}(\cdot)$ denotes the anisotropic equilibrium operator, $\alpha_{K_{\mathrm{anis}}}(\mathbf{r})$ represents the spatially varying anisotropy strength, and $\mathbf{n}(\mathbf{r})$ is the local easy-axis direction.

To efficiently construct the frequency-domain SM under periodic excitation, we approximate $\mathcal{E}$ using a Chebyshev tensor-product expansion. However, using a fixed and full expansion is computationally expensive, whereas aggressive truncation (e.g., single-term) discards high-order content that is crucial for representing nonlinear particle dynamics. We therefore introduce adaptive truncation by retaining the minimal Chebyshev term set whose cumulative energy reaches $\gamma = 0.95$, thereby preserving dominant harmonics while discarding negligible high-order components. This produces a dense, physics-consistent prior $\mathbf{S}_{\mathrm{model}}$ that maintains descriptive power for nonlinear responses while significantly reducing the computational burden.

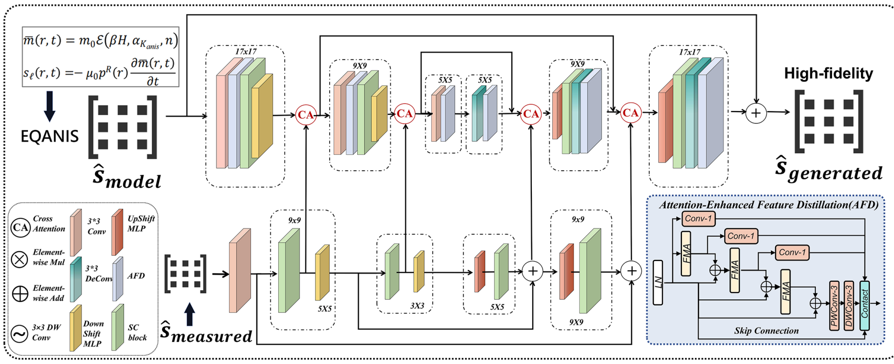

Fig. 2. Overview of P2R-Net for MPI SM calibration. It takes physics-derived $\hat{\mathbf{S}}_{\text{model}}$ and undersampled $\hat{\mathbf{S}}_{\text{measured}}$ as inputs. A dual-branch multi-scale encoder–decoder performs CA fusion, with shared SC-Blocks for voxel-wise coupling and an AFD module in the physics branch to refine anisotropic responses. High-fidelity SM $\hat{\mathbf{S}}_{\text{generated}}$ is output via residual and skip connections.

2.3 P2R-Net Architecture

To address the scale mismatch between the dense physics-derived SM (at the target resolution) and the sparsely measured SM, P2R-Net adopts a dual-branch U-Net style encoder-decoder (Fig. 2) for sparse-to-dense alignment and mapping. The encoder-decoder hierarchy provides multi-resolution features, enabling measurement guidance to be injected from coarse global trends to fine local details. To fuse the two domains without breaking physical structure, we employ cross-attention at matched encoder/decoder levels, where physics-branch features query the measurement branch to selectively retrieve system-specific cues and correct local physics-data misalignment while preserving globally consistent regions. Next, we detail two key components: the SC-Block for voxel-wise coupling modeling and the AFD module for anisotropy-aware correction in the physics branch.

Spatial Shift Convolution Block (SC-Block): MPI SMs exhibit strong voxel-wise spatial coupling due to smooth magnetic field encoding and coil sensitivity profiles. To model this structure with minimal overhead, we introduce the Spatial Shift Convolution Block (SC-Block) as the shared feature extraction unit in both branches. SC-Block follows a lightweight residual pipeline (Conv $\rightarrow$ spatial shift fusion $\rightarrow$ activation $\rightarrow$ Conv + residual): the convolution layers capture local response patterns (e.g., amplitude/phase variations), while the Shift8 operation itself enlarges the local spatial neighborhood without introducing additional learnable parameters. This design is interpretable for MPI-like local magnetic interactions, parameter-efficient for high-dimensional SMs, and stable under deep stacking via residual learning. Concretely, the input feature maps are divided into $G = 8$ channel groups, corresponding to eight spatial directions, i.e., up, down, left, right, upper-left, upper-right, lower-left, and lower-right. Each group is shifted by one pixel along its assigned direction and then aggregated to model neighborhood interactions consistent with the intrinsic spatial correlation of SMs. Zero-padding is used at boundaries to preserve feature size, and the residual connection helps retain fine-grained details.

$$\mathrm{SS}(\boldsymbol{F})_{g,i,j,c} = \boldsymbol{F}_{g,\, i+\Delta i_g,\, j+\Delta j_g,\, c}, \quad (\Delta i_g, \Delta j_g) \in \mathcal{D}, \tag{3}$$

where $\mathcal{D} = \{(-1,0),(1,0),(0,-1),(0,1),(-1,-1),(-1,1),(1,-1),(1,1)\}$; $g \in \{1,\dots,G\}$ denotes the channel group index with $G = 8$, (i,j) are spatial coordinates, and $c \in [1, C/G]$ is the intra-group channel index. Boundary pixels are zero-padded to preserve the feature map size.

Attention-Enhanced Feature Distillation with Frequency Modulation Attention(AFD): Although the anisotropy-aware equilibrium model yields physically consistent SM topology, physics-simulated features may still exhibit local bias and response imbalance due to modeling approximations and unknown system factors. To mitigate this before cross-scale mapping, we apply AFD in the model branch, which combines normalization, channel distillation, attention reweighting, and lightweight feedforward refinement to suppress redundant responses and rebalance feature distributions while avoiding oversmoothing. In addition, AFD integrates Frequency Modulation Attention (FMA) [12], which performs FFT–learnable (1×1) spectral mixing–inverse FFT to enforce tracer-dependent harmonic consistency by enhancing meaningful harmonics and suppressing non-harmonic artifacts. Together, these designs improve quantitative fidelity and robustness of the calibrated SM. This optimized spectral transformation is defined as:

$$\mathbf{A} = \mathrm{Inv}\mathcal{F}\left(\mathrm{Conv}_{1\times1}\left(\mathcal{F}\left(\mathrm{LN}(f_{in})\right)\right)\right), \tag{4}$$

where $\mathcal{F}(\cdot)$ (FFT) maps the Layer-Normalized input from the spatial domain $\mathbb{R}^{H\times W\times C}$ to the frequency spectrum $\mathbb{C}^{H\times\frac{W}{2}\times 2C}$. The subsequent $\mathrm{Conv}_{1\times1}$ acts as a learnable harmonic filter, dynamically amplifying physically significant frequency bands while suppressing non-harmonic noise, before $\mathrm{Inv}\mathcal{F}(\cdot)$ (Inverse FFT) restores the spatial representation.

3 Experiments Results and Discussion

Data preparation and compared methods: We used the public SM13 dataset [9] (CC BY 4.0), acquired on a Bruker preclinical scanner with a Perimag delta-sample over a 17×15 grid (34×30 mm^2 FOV). The measured SMs were zero-padded to 17×17, represented by real/imaginary channels, peak-normalized, and filtered by retaining SNR$>$ 4 frequency components. Sparse inputs were obtained from a fixed deterministic mask, yielding a uniformly sampled 9×9 subset. The data were split into training/testing sets at an

80%/20% ratio before augmentation, resulting in 1600 augmented training samples and 40 independent raw test samples. Evaluation used six phantoms, including three shape targets and three resolution rods. We compared P2R-Net with physics simulators (EQ, FP, EQANIS), supervised SR methods (SRCNN, SMRnet, ISPAnet), and unsupervised baselines (Bilinear, Bicubic, CS, DIP). Supervised training used MSE to the measured SM. Unsupervised training used $\mathcal{L}_{\text{unsup}} = \mathcal{L}_{\text{phys}} + \mathcal{L}_{\text{meas}}$, where $\mathcal{L}_{\text{phys}}$ combines MSE and VGG loss to $\boldsymbol{S}_{\text{model}}$, and $\mathcal{L}_{\text{meas}} = \|\mathcal{D}_{\Omega}(\hat{\boldsymbol{S}}) - \boldsymbol{S}_{\text{sparse}}\|_2^2$ enforces consistency with sparse measurements under the deterministic mask Ω. All learning-based methods used the same split, preprocessing, sampling setting, and reconstruction protocol. Reconstruction was performed using Kaczmarz regularization [10].

Comparisons with State-of-the-Art Methods: Fig. 3 reports both qualitative SM recovery and the downstream MPI reconstruction, together with the corresponding energy-profile evaluations. In the supervised setting (15×17), even the measured SM does not perfectly separate the two phantom rods at this resolution; therefore, the line-profile curves of all methods do not exhibit two fully isolated, sharp peaks. This indicates that the bottleneck is not only recovery accuracy but also the intrinsic resolution limit of low-dimensional SMs. Nevertheless, our P2R-Net produces the closest profile to the measured reference, with reduced sidelobe artefacts and less spurious oscillation around the peak regions, which is also reflected by cleaner SM error maps and more faithful reconstructions along the marked cross-section. These results suggest that P2R-Net improves calibration primarily by suppressing measurement-inconsistent sidelobes and stabilizing amplitude scaling, which are critical for quantitative reconstruction. Quantitatively (Table 1, Comparison), P2R-Net achieves the best SM recovery metrics (nRMSE 0.0559, PSNR 25.97 dB, SSIM 0.9042). This improvement transfers to reconstruction, where we obtain nRMSE 0.0187, PSNR 26.27 dB, and SSIM 0.9724, outperforming all competing baselines in both fidelity and structural similarity.

To obtain a higher-resolution SM for separating closely spaced rods, we further perform unsupervised training to generate 30×34 SMs. As shown in Fig. 3 (middle), P2R-Net yields sharper and more separated SM responses with less background leakage than physics-based models (EQ/EQANIS/FP) and classical baselines (bilinear/bicubic/CS/DIP), leading to cleaner reconstructions where the two rods are more distinguishable. The energy/line-profile curves (Fig. 3, right-bottom) show two clearer peaks with a deeper inter-peak valley and reduced sidelobes, whereas competing methods exhibit peak broadening or elevated inter-peak floors. These results indicate that physics-to-reality mapping can refine high-frequency details from sparse measurements while preserving physical plausibility, improving effective resolution beyond the original measured grid.

Ablation studies: We ablate core components of P2R-Net by removing the SC-Block (MIC), AFD, the physics-driven branch (Branch1), or the measurement-

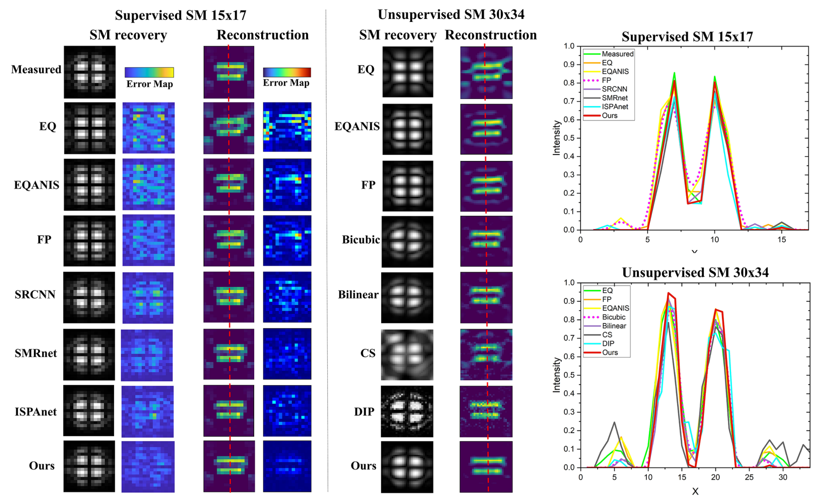

Fig. 3. The visualization results of SMs generation and MPI reconstruction

mapping branch (Branch2). As shown in Table 1, the full model achieves the best SM recovery and reconstruction performance. The dual-branch design is crucial: removing Branch2 causes the largest drop in reconstruction (nRMSE 0.0187 $\rightarrow$ 0.0309, $\sim$65%), highlighting the importance of sparse real measurements for correcting system-specific mismatch, while removing Branch1 also degrades SM fidelity (nRMSE 0.0559 $\rightarrow$ 0.0823), indicating the physics prior stabilizes recovery under sparse observations. SC-Block and AFD provide complementary refinements, yielding moderate but consistent gains by modeling voxel-wise coupling and mitigating simulation-feature bias, respectively.

Table 1. Quantitative comparison and ablation results for system matrix recovery and the corresponding MPI reconstruction on 15×17 SMs.

Category	Methods	SM Recovery			Reconstruction		
		nRMSE ↓	PSNR ↑	SSIM ↑	nRMSE ↓	PSNR ↑	SSIM ↑
Comparison	EQ	0.1185	19.37	0.6623	0.0443	18.79	0.8047
	EQANIS	0.0991	20.97	0.7481	0.0287	22.65	0.9138
	FP	0.0975	21.13	0.7558	0.0283	22.77	0.9179
	SRCNN	0.1024	20.36	0.7516	0.0365	20.45	0.9008
	SMRnet	0.0688	23.89	0.8734	0.0269	23.00	0.9479
	ISPAnet	0.0775	22.84	0.8269	0.0316	21.71	0.9213
	Ours	**0.0559**	**25.97**	**0.9042**	**0.0187**	**26.27**	**0.9724**
Ablation	W/O MIC	0.0770	22.96	0.8564	0.0226	24.68	0.9571
	W/O AFD	0.0689	24.09	0.8656	0.0195	25.80	0.9693
	W/O Branch1	0.0823	22.31	0.8248	0.0244	23.98	0.9313
	W/O Branch2	0.0844	22.06	0.8176	0.0309	21.91	0.9263

4 Conclusion

In this work, we propose P2R-Net, a Physics-to-Reality mapping network with sparse measurement guidance for high-precision MPI reconstruction, aimed at bridging the gap between physics- and measurement-domain SMs under practical calibration constraints. It adopts dual-branch encoder–decoder with multi-scale cross-attention, and incorporates SC block and AFD module for structure-aware refinement. Extensive supervised and unsupervised experiments demonstrate that P2R-Net improves SM fidelity and consistently enhances downstream MPI reconstruction, providing an efficient alternative to time-consuming full-volume calibration. Future work will focus on its adaptability for clinical translation and broader biomedical imaging applications.

Acknowledgments. This study was funded by the National Natural Science Foundation of China under Grants 12271434, 62271394, 62201459; The Scientific and Technological projects of Xi'an under Grant 201805060ZD11CG44; The Scientific and Technology New Star in Shaanxi Province of China under Grant 2023KJXX-035; General Project of the Key Research and Development Plan of Shaanxi Province under Grant 2025SF-YBXM-240; Natural Science Basic Research Plan in Shaanxi Province of China under Grant 2023-JC-JQ-57; Artificial intelligence empowers the team of "scientists + engineers" in education under 2024JH-KGDW-0084.

Disclosure of Interests. The authors have no conflicts to disclose.

References

1. Albers, H., Kluth, T., Knopp, T.: Simulating magnetization dynamics of large ensembles of single domain nanoparticles: Numerical study of brown/néel dynamics and parameter identification problems in magnetic particle imaging. Journal of Magnetism and Magnetic Materials **541**, 168508 (2022)
2. Atalay Aydın, V., Möddel, M., Knopp, T.: Wavelet-based compressed sensing of the system matrix for magnetic particle imaging. Signal, Image and Video Processing **19**(9), 689 (2025)
3. Baltruschat, I.M., Szwargulski, P., Griese, F., Grosser, M., Werner, R., Knopp, T.: 3d-smrnet: Achieving a new quality of mpi system matrix recovery by deep learning. In: Medical Image Computing and Computer Assisted Intervention–MICCAI 2020: 23rd International Conference, Lima, Peru, October 4–8, 2020, Proceedings, Part II 23. pp. 74–82. Springer (2020)
4. Grosser, M., Möddel, M., Knopp, T.: Using low-rank tensors for the recovery of mpi system matrices. IEEE transactions on computational imaging **6**, 1389–1402 (2020)
5. Güngör, A., Askin, B., Soydan, D.A., Saritas, E.U., Top, C.B., Çukur, T.: Transms: Transformers for super-resolution calibration in magnetic particle imaging. IEEE Transactions on Medical Imaging **41**(12), 3562–3574 (2022)
6. Gungor, A., Top, C.B.: Super-resolving reconstruction technique for mpi. International Journal on Magnetic Particle Imaging IJMPI **6**(2 Suppl 1) (2020)

7. Kasson, J.M., Nin, S.I., Plouffe, W., Hafner, J.L.: Performing color space conversions with three-dimensional linear interpolation. Journal of Electronic Imaging **4**(3), 226–250 (1995)
8. Kluth, T.: Mathematical models for magnetic particle imaging. Inverse Problems **34**(8), 083001 (2018)
9. Knopp, T., Scheffler, K.: MPIData: EquilibriumModelWithAnisotropy (2 2024). https://doi.org/10.5281/zenodo.10646064
10. Knopp, T., Rahmer, J., Sattel, T.F., Biederer, S., Weizenecker, J., Gleich, B., Borgert, J., Buzug, T.M.: Weighted iterative reconstruction for magnetic particle imaging. Physics in medicine & biology **55**(6), 1577 (2010)
11. Knopp, T., Weber, A.: Sparse reconstruction of the magnetic particle imaging system matrix. IEEE transactions on medical imaging **32**(8), 1473–1480 (2013)
12. Li, F., Cong, R., Wu, J., Bai, H., Wang, M., Zhao, Y.: Srconvnet: A transformer-style convnet for lightweight image super-resolution. International Journal of Computer Vision **133**(1), 173–189 (2025)
13. Liao, F., Li, M., Feng, W., Xu, Y., Zhang, T., Wu, Z., Hui, H., Zheng, J., Tian, J.: Modeling real-world mpi system matrices from sparse observations. IEEE Transactions on Computational Imaging (2025)
14. Maass, M., Kluth, T., Droigk, C., Albers, H., Scheffler, K., Mertins, A., Knopp, T.: Equilibrium model with anisotropy for model-based reconstruction in magnetic particle imaging. arXiv preprint arXiv:2403.00602 (2024)
15. Malyala[1], A., Zhang, Z., Wang, C., Qin, C.: Sampling-pattern-agnostic mri reconstruction through adaptive consistency enforcement with diffusion. In: Statistical Atlases and Computational Models of the Heart. Workshop, CMRxRecon and MBAS Challenge Papers.: 15th International Workshop, STACOM 2024, Held in Conjunction with MICCAI 2024, Marrakesh, Morocco, October 10, 2024, Revised Selected Papers. p. 140. Springer Nature (2025)
16. Schlereth, M., Schillinger, M., Breininger, K.: Faster, self-supervised super-resolution for anisotropic multi-view mri using a sparse coordinate loss. In: International Conference on Medical Image Computing and Computer-Assisted Intervention. pp. 172–182. Springer (2025)
17. Sun, S., Chen, Y., Zhao, M., Xu, L., Zhong, J.: Image reconstruction for magnetic particle imaging based on sparse representation and deep learning. IEEE Transactions on Instrumentation and Measurement (2024)
18. Weber, A., Knopp, T., et al.: Reconstruction of the magnetic particle imaging system matrix using symmetries and compressed sensing. Advances in Mathematical Physics **2015** (2015)
19. Yang, X., Shao, G., Zhang, Y., Wang, W., Qi, Y., Han, S., Li, H.: Applications of magnetic particle imaging in biomedicine: Advancements and prospects. Frontiers in physiology **13**, 898426 (2022)
20. Yin, L., Guo, H., Zhang, P., Li, Y., Hui, H., Du, Y., Tian, J.: System matrix recovery based on deep image prior in magnetic particle imaging. Physics in Medicine & Biology **68**(3), 035006 (2023)
21. Zhang, L., Li, J., Du, J., Fang, G., Zhang, D., Tang, Z., Guo, H., He, X.: Current reconstruction approaches of magnetic particle imaging: A review. Journal of Magnetism and Magnetic Materials p. 171894 (2024)
22. Zhang, L., Li, J., He, X., Tang, Z., Li, S., Zhao, Y., Guo, H.: Iterative up-and-down sampling network based on pyramid pooling and attention mechanism for 3d system matrix recovery in mpi. IEEE Transactions on Instrumentation and Measurement (2025)

23. Zhu, T., Yin, L., He, J., Wei, Z., Yang, X., Tian, J., Hui, H.: Accurate concentration recovery for quantitative magnetic particle imaging reconstruction via nonconvex regularization. IEEE Transactions on Medical Imaging (2024)